## Role of metastable charge states in a quantum-dot spin-qubit readout

Mason, J. D.; Studenikin, S. A.; Kam, A.; Wasilewski, Z. R.; Sachrajda, A. S.; Kycia, J. B.



**Publisher's version / Version de l'éditeur:**
https://doi.org/10.1103/PhysRevB.92.125434
*Physical Review. B, Condensed Matter and Materials Physics, 92, 12, 2015-09-15*

PHYSICAL REVIEW B **92**, 125434 (2015)

# Role of metastable charge states in a quantum-dot spin-qubit readout

J. D. Mason,[1] S. A. Studenikin,[2] A. Kam,[2] Z. R. Wasilewski,[2,*] A. S. Sachrajda,[2] and J. B. Kycia[1,†]
[1]*Department of Physics and Astronomy, University of Waterloo, Waterloo, ON N2L 3G1, Canada*
[2]*National Research Council Canada, Ottawa, ON K1A 0R6, Canada*
(Received 8 July 2015; revised manuscript received 3 September 2015; published 25 September 2015)

Readout of a spin qubit in a lateral gate-defined quantum-dot device typically involves a charge detector and a spin-to-charge conversion technique employing spin blockade. We investigate alternative mechanisms for spin-to-charge conversion involving metastable excited charge states made possible by an asymmetry in the tunneling rates to the leads. This technique is used to observe Landau-Zener-Stückelberg oscillations of the S-$T_+$ qubit within the (1,0) ground state region of the charge stability diagram. The oscillations are $\pi$ phase shifted relative to those detected using the standard technique and display a nonsinusoidal waveform due to the increased relaxation time from the metastable state.

DOI: 10.1103/PhysRevB.92.125434 PACS number(s): 73.23.Hk, 73.63.Kv

## I. INTRODUCTION

Quantum-dot devices attract wide interest as promising candidates for spin qubits in quantum-information applications [1]. Of recent interest is the formation and manipulation of coherent superpositions of spin states using the Landau-Zener-Stückelberg (LZS) approach [2–9]. Observation of spin state LZS oscillations within the charge stability diagram of a quantum-dot device involves a projective measurement in the qubit basis states. Such a spin state readout requires a spin-to-charge conversion mechanism, typically employing the spin blockade phenomenon [10], by which each spin state is mapped to a unique charge state followed by a charge state measurement using a nearby electric field sensor such as a quantum point contact (QPC) [11,12].

We concentrate on the two-electron spin qubit formed by the singlet, S(1,1), and the $m_s = 1$ triplet, $T_+(1,1)$, in a double quantum dot (DQD) [3]. After placing the qubit in a superposition of these states, its evolution occurs in the (1,1) ground state region of the stability diagram. Following this qubit manipulation, gate voltages are rapidly adjusted to change the ground state of the system from (1,1) to (2,0). Readout of the qubit spin state occurs in this regime. The S(1,1) and S(2,0) states are tunnel coupled allowing for a fast transition between these two configurations. The transition from $T_+(1,1)$ to S(2,0) is, however, inhibited due to spin blockade. With T(2,0) energetically inaccessible due to the exchange interaction, $T_+(1,1)$ remains in an excited state for a relaxation time $T_1$. By choosing a measurement time, $T_m$, satisfying $T_m < T_1$, this conventional technique maps the qubit spin states S(1,1) and $T_+(1,1)$ to the charge states (2,0) and (1,1) respectively. These charge states, and thus the corresponding spin states, are easily distinguished using a charge detector such as a QPC. An alternative to this spin-to-charge conversion technique has recently been demonstrated [13]. It involves mapping $T_+(1,1)$ to the (2,1) metastable excited state in the (2,0) ground state regime. In this work, we perform a more detailed study of spin-to-charge conversion mechanisms employing metastable states in a DQD with asymmetric couplings to the leads. We use LZS oscillations of the S-$T_+$ qubit to demonstrate a spin-to-charge conversion mechanism involving the (1,0) metastable state within the (2,0) ground state regime. We also show that a metastable state can be employed to readout the spin state of this qubit within the (1,0) ground state regime.

## II. EXPERIMENTAL DETAILS

An electron micrograph of the device used to realize the spin qubit is shown in the inset of Fig. 1(a). The DQD potential wells and QPC charge detectors are formed in the two-dimensional electron gas (2DEG) of a GaAs/AlGaAs heterostructure by applying negative voltages to the TiAu depletion gates. The 2DEG which is 90 nm below the surface has density $2.1 \times 10^{11}$ cm$^{-2}$ and mobility $1.7 \times 10^6$ cm$^2$/V s. A magnetic field of 80 mT is applied in the plane of the 2DEG perpendicular to the line connecting the two dots. This choice of field direction minimizes the effect of spin-orbit coupling on the energy splitting between the S and $T_+$ states [14]. To mitigate telegraph noise problems, 0.25 V bias is applied to all gates while cooling the device from room temperature to the base temperature of the dilution refrigerator [15]. The top right side QPC is used to detect changes in the charge state of the DQD. To be maximally sensitive to these changes, the QPC conductance is set to 0.3 $e^2$/h. We measure transconductance, $dI_{\mathrm{QPC}}/dV_1$, by applying a constant 200 $\mu$V bias across the QPC and a 240 $\mu V_{\mathrm{rms}}$, 17 Hz signal to gate 1 [16]. The resulting oscillating QPC current is detected using a room temperature I-V converter and a lock-in amplifier. A charge stability diagram acquired using this technique is shown in Fig. 1(a). Transconductance minima (black) and maxima (white) divide the diagram into charge stable regions labeled ($N_L$,$N_R$) with $N_L$ ($N_R$) electrons occupying the left (right) dot. Extensions of charging lines shown as dashed lines (yellow) further divide the (2,0) region into parts labeled R1, R2, and R4. These three regions and the (1,0) region labeled R3 each correspond to a different ordering of the energy levels of the charge states (1,0), (2,0), (1,1), and (2,1) as shown in Fig. 4 and discussed below.

Figure 1(b) shows the energy levels of the S and $T_+$ states as a function of detuning [3]. The detuning axis is represented

*Present address: Department of Electrical and Computer Engineering, University of Waterloo, Waterloo, Ontario, Canada.
†Corresponding author: jkycia@uwaterloo.ca

 

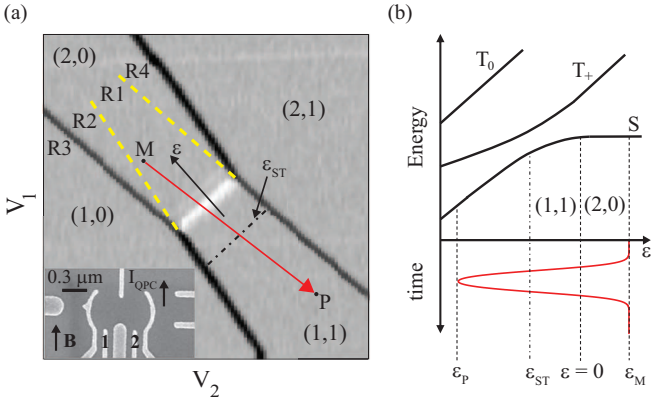


FIG. 1. (Color online) (a) Gray scale plot of the transconductance of the QPC charge detector in the few electron regime of the DQD. The diagram is divided into charge stable regions labeled ($N_L$,$N_R$). Charging lines (black) and extensions of charging lines (yellow dash) form boundaries between the regions labeled R1, R2, R3, and R4. Inset: Scanning electron micrograph of the DQD gate layout. The high bandwidth gates are labeled 1 and 2. The QPC used in the transconductance measurements is indicated with an arrow labeled $I_{QPC}$. The 80 mT magnetic field is applied in the direction of the arrow labeled **B**. (b) Energy level diagram of the two-electron spin states showing the avoided crossing involving the S and $T_+$ qubit states [dash-dot in (a)]. Below this diagram is shown a Gaussian pulse. Such pulses are applied to gates 1 and 2 to produce the trajectory represented by the arrow connecting points M and P in (a).

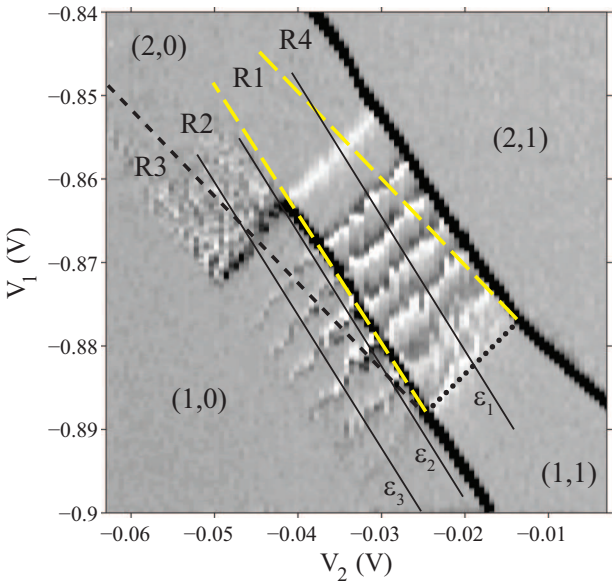


FIG. 2. (Color online) Stability diagram of the DQD acquired in the presence of a gate pulse (lock-in amplifier time constant 1 s). The pulse has a width of 17 ns, a rise time of 8 ns, and a period of 2 $\mu$s. The black short-dashed line indicates the position of the missing charging line separating the (1,0) and (2,0) ground state regions. This line together with the extensions of charging lines (yellow long-dash) divide the diagram into regions labeled R1, R2, R3, and R4 as in Fig. 1(a). Spin state readout is accomplished using a metastable charge state in regions R2 and R3. The position of the (2,0) $\leftrightarrow$ (1,1) charge transfer line is indicated with a black dotted line. The lines labeled $\varepsilon_1$, $\varepsilon_2$, and $\varepsilon_3$ indicate the positions of the line scans relevant to Fig. 5.

by a black arrow labeled $\varepsilon$ in Fig. 1(a). The charge transfer line (white) between the (2,0) and (1,1) ground state regions corresponds to $\varepsilon = 0$. The DQD electrons interact with the gallium and arsenic nuclei leading to the avoided crossing in the (1,1) region at $\varepsilon = \varepsilon_{ST}$ [3,17,18]. Below the energy level diagram is sketched a typical Gaussian pulse used in this work. The corresponding trajectory, chosen to be nearly parallel to the left dot charging lines in order to reach the new regime discussed below, is represented by an arrow connecting points M and P in Fig. 1(a). Starting in the (2,0) ground state region at point M, a gate voltage pulse sweeps the system into the (1,1) region through the avoided crossing to point P, in the process creating a superposition of the qubit states. This superposition evolves during the segment of the pulse spent in the (1,1) ground state region beyond the avoided crossing. The second half of the pulse returns the system to the (2,0) region for readout of the final spin state at point M using the QPC charge detector and a spin-to-charge conversion technique. The voltage pulse components are applied to gates 1 and 2 via bias tees using two synchronized channels of an arbitrary waveform generator [19]. The pulse is a numerical convolution of a rectangular pulse and a Gaussian function giving it a rise time of 8 ns (10% to 90%).

## III. LANDAU-ZENER-STÜCKELBERG OSCILLATIONS

A Gaussian voltage pulse with duration $\tau = 17$ ns (FWHM) is applied every $T_m = 2$ $\mu$s during the acquisition of a stability diagram to produce the LZS oscillations displayed in Fig. 2. The device is tuned in a specific regime to have very asymmetric tunneling couplings to the leads. The right dot is coupled to the right lead with a corresponding tunneling rate of greater than 20 MHz [20]. Unlike in the case of Fig. 1(a), the left dot is comparatively weakly coupled to the left lead with a tunneling rate of less than the 17 Hz modulation frequency as evidenced by the missing charging line between the (1,0) and (2,0) regions (black short-dash). We identify oscillations in regions R1, R2, R3, and R4. For region R1, the oscillations are contained within the boundaries (yellow) shown in Fig. 3(a). The arrow indicates a pulse which just reaches the S-$T_+$ avoided crossing. For initial points within the boundaries, a similar pulse trajectory sweeps through the avoided crossing resulting in the observed LZS oscillations. In region R1, (2,0) is the ground state while (1,1) and (1,0) are excited states as shown in Fig. 4(a). The relaxation time from the $T_+$(1,1) excited state to the S(2,0) ground state, $T_1$, is estimated by measuring the decay of the positive transconductance signal (white fringes) as the time between pulses, $T_m$, is increased (not shown). With a relaxation time $T_1 \sim 50$ $\mu$s and a comparatively short measurement time $T_m = 2$ $\mu$s, the phenomenon of spin blockade is used to achieve spin-to-charge conversion in the manner discussed above.

## IV. ROLE OF METASTABLE CHARGE STATES

Entering region R2 from R1 in Fig. 2 involves crossing the extension of the right dot charging line separating the (1,0) and (1,1) ground state regions (yellow long-dash). This makes

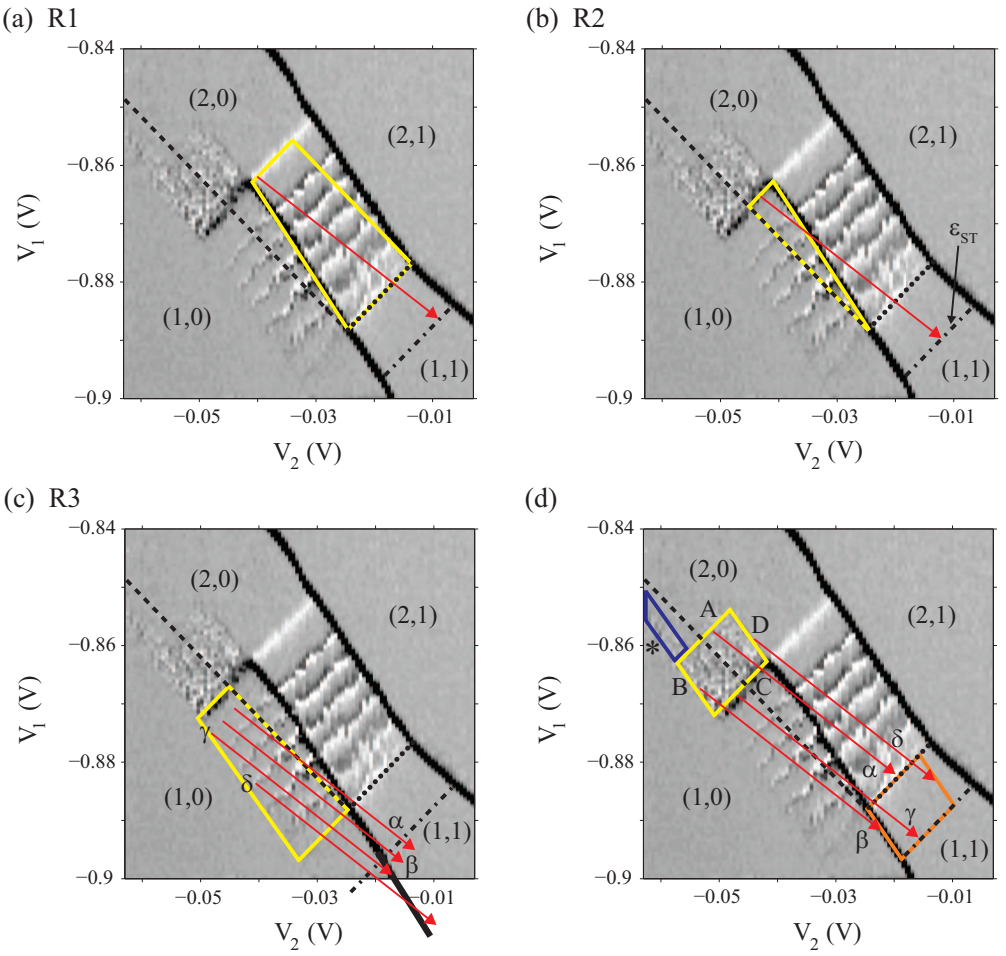


FIG. 3. (Color online) The LZS oscillations in regions R1, R2, and R3 are outlined (yellow) in (a), (b), and (c) respectively. Arrows indicate examples of pulse trajectories. The (1,0) ↔ (2,0) charging line and the (2,0) ↔ (1,1) charge transfer line are shown as dashed and dotted lines, respectively. The position of the S-$T_+$ avoided crossing is indicated with a dash-dotted line. (d) Regions of telegraph noise resulting from fluctuations between the (1,0) and (2,0) charge states are outlined in yellow (boundaries A–D) and blue (∗).

(1,0) the first excited state while (2,0) remains the ground state as shown in Fig. 4(b). The oscillations in this region are contained within the highlighted (yellow) triangular area of Fig. 3(b). Readout of S(1,1) involves a rapid transition to the S(2,0) ground state as in R1. Readout of $T_+(1,1)$, however, involves the use of the metastable excited state (1,0) which is made possible by the asymmetry in the tunneling rates to the leads. After the pulse, upon return to the (2,0) ground state region, an electron is ejected from the right dot and $T_+(1,1)$ transitions to the (1,0) charge state on a time scale, $T_R$, that is short relative to $T_1$. The corresponding tunnel rate being $\Gamma_R > 20$ MHz implies a tunneling time $T_R < 50$ ns. Due to the weak coupling of the left dot to its lead, the (1,0) state is metastable for $T_L > 50$ ms. Importantly $T_L > T_m$ and as a result $T_+(1,1)$ is effectively mapped to the (1,0) charge state during the measurement period.

Crossing the left dot charging line separating the (1,0) and (2,0) ground state regions (black short-dashed line in Fig. 2) in the process of moving from R2 to R3, makes (1,0) the ground state and (2,0) the first excited state as shown in Fig. 4(c). The (1,1) charge configuration remains the second excited state. The corresponding LZS oscillations are outlined (yellow) in Fig. 3(c). Readout of a spin state is performed in R3 using a new spin-to-charge conversion mechanism that employs another metastable state. After a pulse, since $T_R \ll T_1$, an electron is ejected from the right dot and $T_+(1,1)$ transitions to the (1,0) ground state before it can decay to the first excited state, S(2,0). For the singlet state, as in R1 and R2, an electron is transferred from the right dot to the left dot and S(1,1) transitions to S(2,0). In R3, the difference is that S(2,0) is a metastable excited state due to the long tunneling time for the left dot, $T_L$. As in region R2, the use of this metastable state is possible because it is long-lived relative to the measurement period, $T_m$. Since the involved charge states (2,0) and (1,0) differ by one electron, we expect after optimization (which has not been accomplished in this work), a larger signal contrast in R3 as compared to R1 [13].

Figure 4(d) shows the arrangement of energy levels corresponding to region R4 of Fig. 2. Charge state (2,0) is the ground state while (2,1) and (1,1) are excited states. In this case, the $T_+(1,1)$ qubit state decays to the S(2,0) ground state in a time $T_1$ which is short relative to the lead tunneling time for the left dot, $T_L$, required for the transition between the (1,1) and (2,1) excited states. Essentially the excited state (2,1) does

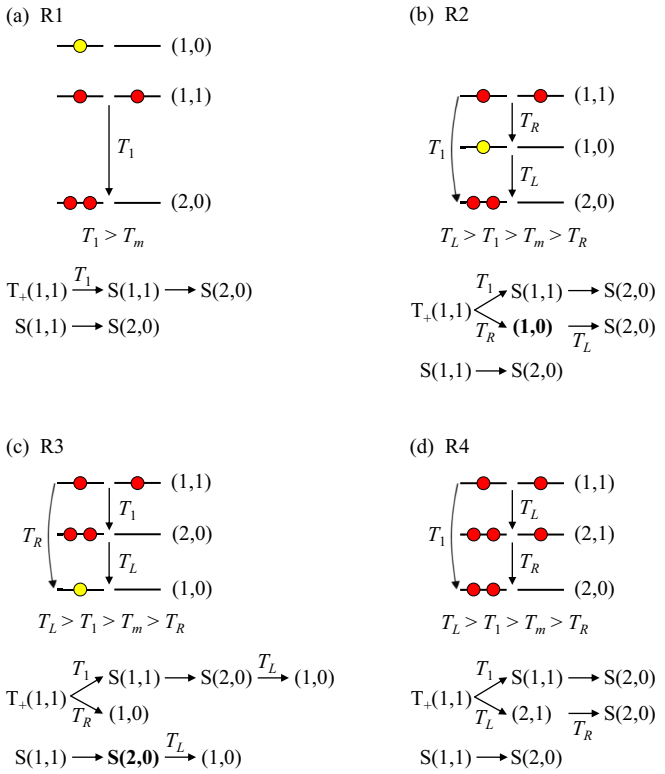


FIG. 4. (Color online) Schematic energy diagram for each of the four regions R1–R4 shown in Fig. 2. The processes by which each of the qubit states, S(1,1) and $T_+(1,1)$, eventually transitions to the ground state are also shown (metastable states in bold). The mechanism of spin-to-charge conversion in each region relies on mapping one of the qubit spin states to an excited charge state that is long-lived relative to the readout measurement time, $T_m$. (a) Region R1: Standard readout of the S-$T_+$ qubit. The S(1,1) state transitions to the S(2,0) singlet ground state while $T_+(1,1)$ remains in the (1,1) excited charge state for a time $T_1$ due to spin blockade. (b) Region R2: Metastable excited state used in the readout. Due to the strong coupling of the right dot to its lead, an electron is rapidly ejected from the right dot and $T_+(1,1)$ transitions to the (1,0) charge state. This excited state is metastable due to the slow tunnel rate between the left dot and the leads, $T_L$. (c) Region R3: Metastable excited state and single electron ground state used in the readout. The $T_+(1,1)$ state transitions to the (1,0) ground state due to the strong coupling of the right dot to its lead and S(1,1) transitions to the S(2,0) metastable excited state. (d) Region R4: The (2,1) first excited state is not metastable for our choice of lead couplings and as a result plays no role in the spin-to-charge conversion mechanism.

not play a role in spin-to-charge conversion in this region and the LZS oscillations appear identical to those in region R1. For a different choice of lead tunneling couplings, the (2,1) excited state could become a metastable charge state and be used in the spin state readout as demonstrated in Ref. [13].

In regions R2 and R3, readout of $T_+(1,1)$ involves the single electron state (1,0). Once (1,0) is occupied in the course of spin-to-charge conversion, a mechanism is required to add an electron to the DQD for LZS processes to begin again. In region R2, the system either decays to the (2,0) ground state during the period between pulses or transitions to the (1,1) state during the segment of a pulse spent in the (1,1) ground state region. The latter mechanism being possible because the tunneling time between the right dot and its lead, $T_R < 50$ ns, is comparable to or less than the pulse duration, $\tau = 17$ ns. For region R3, with (1,0) being the ground state, adding an electron must result from a pulse entering the (1,1) ground state region as is the case for the pulses labeled $\alpha$ and $\beta$ in Fig. 3(c). Entering the (2,0) ground state region during pulse $\alpha$ is unlikely to load an electron into the DQD because the tunneling time between the left dot and its lead is long relative to the pulse duration. Note that the oscillations stop at the lower left boundary of R3 because the pulse labeled $\gamma$ just reaches the charging line between the (1,0) and (1,1) ground state regions. For initial points to the left of this boundary, an electron cannot be added to the right dot during a pulse.

Consider the pulse labeled $\delta$ in Fig 3(c). For trajectories of this type, which start near the lower left boundary of R3, the system sweeps through an extension [into the (1,0) ground state region] of the S-$T_+$ avoided crossing. The existence of LZS oscillations near the lower left boundary, which run parallel to those in the rest of the stability diagram, indicates that an avoided crossing of the S and $T_+$ spin states of the excited charge state (1,1) exists within the (1,0) ground state region.

Figure 5 shows plots of transconductance as a function of detuning and pulse duration. The vertical axes are projections onto the $V_1$ axis of the lines labeled $\varepsilon_1$, $\varepsilon_2$, and $\varepsilon_3$ in Fig. 2. Note the $\pi$ phase shift of the oscillations in R2 and R3 as compared to those of R1. This results from the use of the metastable state (1,0) for spin-to-charge conversion in R2 and R3 in the following way. The values of QPC charge detector current corresponding to the three involved charge states (1,0), (2,0), and (1,1) are $I(1,0)$, $I(2,0)$, and $I(1,1)$, respectively. With the charge detector closer to the right dot than the left dot, the current values have the relationship $I(1,0) > I(2,0) > I(1,1)$. In region R1, a change from measuring a singlet to a triplet state creates a change in QPC current $\Delta I_{\mathrm{QPC}} = I(1,1) - I(2,0) < 0$ while in regions R2 and R3, the resulting change is $\Delta I_{\mathrm{QPC}} = I(1,0) - I(2,0) > 0$. It is this difference in the sign of $\Delta I_{\mathrm{QPC}}$ that leads to a difference in the sign of the transconductance signal, $dI_{\mathrm{QPC}}/dV_1$, producing the observed $\pi$ phase shift evident in Figs. 2 and 5.

Line scans taken at the positions of the dashed lines in Figs. 5(a), 5(c), and 5(e) ($\tau = 17$ ns) are displayed in Figs. 5(b), 5(d), and 5(f). The oscillations in region R1 are quasisinusoidal while in R2 and R3, they appear as comparatively sharp peaks and dips. Note that every pixel of Fig. 2 is the average of $5 \times 10^4$ measurements each of which is made during the $T_m = 2$ $\mu$s period between pulses. Prior to each of these Gaussian pulses, however, there is no step which initializes the system to a particular state. In the case of R1, for example, consider the situation after the measurement of $T_+(1,1)$. Relaxation to the S(2,0) ground state may occur before the next pulse but since $T_m < T_1$, the system may not have time to decay. Consequently the next pulse could begin with the system still in $T_+(1,1)$. It has recently been shown that LZS oscillations of a nonsinusoidal waveform can be produced when $T_m \ll T_1$ in cases without applied initialization [21]. For region R1 though, $T_m/T_1 \sim 0.04$ and the oscillations still appear nearly sinusoidal. The effect seems pronounced, however, in regions R2 and R3. In these cases, the relaxation

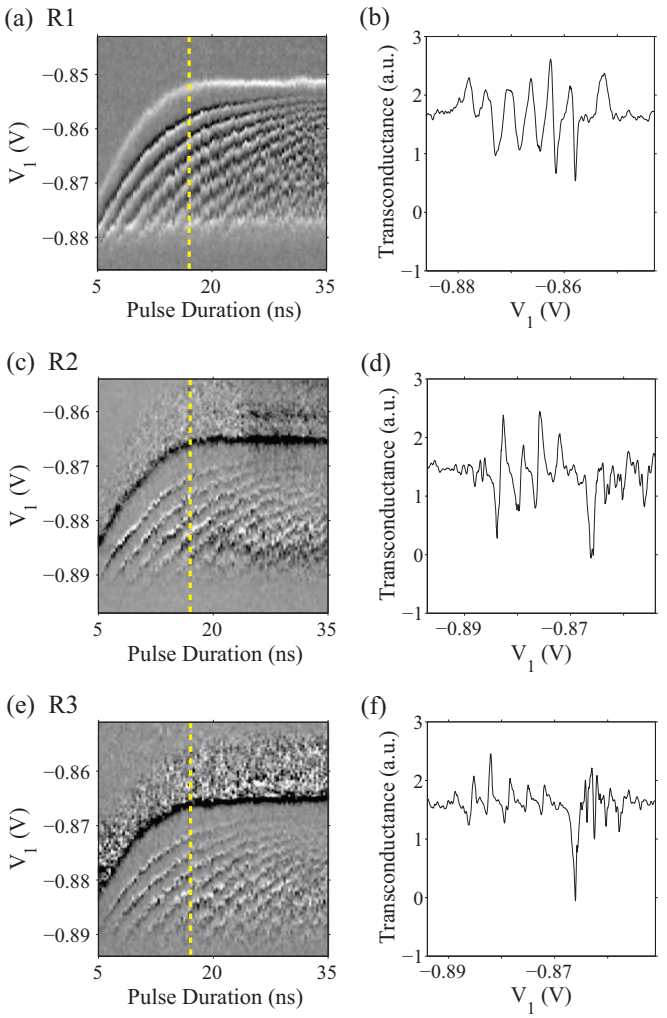


FIG. 5. (Color online) Plots of transconductance as a function of initial detuning along $V_1$ and pulse duration for regions R1 (a), R2 (c), and R3 (e) (lock-in amplifier time constant 300 ms). The vertical axes correspond to projections onto the $V_1$ axis of the trajectories shown as black lines labeled $\varepsilon_1$, $\varepsilon_2$, and $\varepsilon_3$ in Fig. 2 (differences between the vertical axis gate voltages and those expected from Fig. 2 are due to device drift). (b), (d), and (f) Line scans through the data of (a), (c), and (e) taken at the positions of the vertical dashed lines.

time in R1, $T_1$, associated with coupling to the nuclear spin bath, is replaced by the much longer metastable relaxation time $T_L$. With $T_m/T_L \sim 10^{-5}$, the nonsinusoidal waveform is clearly apparent.

## V. TELEGRAPH NOISE REGION

We observe telegraph noise within regions R2 and R3 in Fig. 2. A detailed description of the processes involved in the generation of the noise will be given elsewhere. Here we limit ourselves to a general outline. A bounded noise region can result from the absorption of phonons produced by a biased QPC charge detector [22]. In our case, however, it is a consequence of the Gaussian pulses. Figure 3(d) shows the boundaries (yellow) of the noise region (A–D) mapped by the pulses (arrows) to an area (orange) within the (1,1) ground state region of the stability diagram that lies between the charge transfer line (dot) and the S-$T_+$ avoided crossing (dash-dot). The noise spans across both R2 and R3 regions. The underlying mechanism involves transitions between the (2,0) and (1,0) charge states for both regions. Consider R3, for example, where (1,0) is the ground state and (2,0) is the metastable first excited state. The metastable state slows transitions to the ground state making the noise observable using our low-bandwidth charge detection technique. To occupy the (2,0) state requires first a transition from (1,0) to (1,1) during the pulse [in the orange outlined area in the (1,1) region of Fig. 3(d)] when either T(1,1) or S(1,1) is formed. If the state is T(1,1), then the system will relax to (1,0) after the pulse. However, the state S(1,1) will transition to the (2,0) metastable charge state. Since S(1,1) and T(1,1) occur randomly, the noise is observed. The noise stops when the pulse either cannot reach into the (1,1) region or when the pulse sweeps across the S-$T_+$ avoided crossing and LZS oscillations begin. This is observed at boundaries A and C, respectively. Pulse $\alpha$ connects boundary A to the charge transfer line and pulse $\gamma$ connects boundary C to the S-$T_+$ avoided crossing. Consider boundary B. Pulse $\beta$ connects this boundary to the right dot charging line separating the (1,0) and (1,1) ground state regions. At this charging line, the (1,0) and (1,1) states are degenerate and the pulse therefore provides a means by which the system can transition out of the (1,0) ground state of R3 and into the intermediate (1,1) second excited state. Note that the pulse continues to reach the charging line for initial points up the $V_1$ axis and as a result, noise is observed within the outlined (blue) region labeled with an asterisk. Finally, consider boundary D. It runs along the extension of the charging line between the (1,0) and (1,1) regions and pulse $\delta$ connects it to the area between the charge transfer line and the S-$T_+$ avoided crossing. To the right of this boundary, there is no long-lived metastable state, so any fluctuations are suppressed due to fast relaxation to the ground state.

## VI. CONCLUSIONS

In conclusion, we have studied the role of metastable charge states for spin state readout. We employed LZS oscillations of the S-$T_+$ qubit in this study, though the results are applicable for readout of any other spin qubits, for example, S-$T_0$ [2,4,23,24] or exchange-only [25,26] qubits. In two distinct regions of the charge stability diagram, the conventional spin-to-charge conversion mechanism involving the (1,1) and (2,0) charge states is replaced by a mechanism involving a metastable charge state. In these cases, the qubit spin states are instead mapped to the (1,0) and (2,0) charge states. This technique has led to the observation of LZS oscillations within a new regime where (1,0) is the ground state. We have also shown that the combination of a spin-to-charge conversion mechanism involving a metastable state and a pulse without an initialization step can produce LZS oscillations having a nonsinusoidal waveform.

It has been shown in Ref. [13] that schemes that take advantage of metastable states can result in an enhanced contrast between charge states used in the spin-to-charge conversion process. We have studied a DQD in which one dot is weakly coupled to the leads, resulting in a number

of metastable states. As spin-qubit circuits incorporate more quantum dots, metastable charge states resulting from the unavoidable near isolation of inner dot electrons will become more common and the resultant consequences such as those we report will need to be taken into account.

**ACKNOWLEDGMENTS**

We acknowledge useful discussions with Hugo Ribeiro, Bill Coish, and Aashish Clerk. J.B.K. acknowledges funding from NSERC.

[1] D. Loss and D. P. DiVincenzo, Phys. Rev. A **57**, 120 (1998).
[2] J. R. Petta, A. C. Johnson, J. M. Taylor, E. A. Laird, A. Yacoby, M. D. Lukin, C. M. Marcus, M. P. Hanson, and A. C. Gossard, Science **309**, 2180 (2005).
[3] J. R. Petta, H. Lu, and A. C. Gossard, Science **327**, 669 (2010).
[4] O. E. Dial, M. D. Shulman, S. P. Harvey, H. Bluhm, V. Umansky, and A. Yacoby, Phys. Rev. Lett. **110**, 146804 (2013).
[5] L. Gaudreau, G. Granger, A. Kam, G. C. Aers, S. A. Studenikin, P. Zawadzki, M. Pioro-Ladrière, Z. R. Wasilewski, and A. S. Sachrajda, Nat. Phys. **8**, 54 (2012).
[6] H. Ribeiro and G. Burkard, Phys. Rev. Lett. **102**, 216802 (2009).
[7] H. Ribeiro, J. R. Petta, and G. Burkard, Phys. Rev. B **82**, 115445 (2010).
[8] H. Ribeiro, J. R. Petta, and G. Burkard, Phys. Rev. B **87**, 235318 (2013).
[9] H. Ribeiro, G. Burkard, J. R. Petta, H. Lu, and A. C. Gossard, Phys. Rev. Lett. **110**, 086804 (2013).
[10] K. Ono, D. G. Austing, Y. Tokura, and S. Tarucha, Science **297**, 1313 (2002).
[11] M. Field, C. G. Smith, M. Pepper, D. A. Ritchie, J. E. F. Frost, G. A. C. Jones, and D. G. Hasko, Phys. Rev. Lett. **70**, 1311 (1993).
[12] R. Hanson, L. P. Kouwenhoven, J. R. Petta, S. Tarucha, and L. M. K. Vandersypen, Rev. Mod. Phys. **79**, 1217 (2007).
[13] S. A. Studenikin, J. Thorgrimson, G. C. Aers, A. Kam, P. Zawadzki, Z. R. Wasilewski, A. Bogan, and A. S. Sachrajda, Appl. Phys. Lett. **101**, 233101 (2012).
[14] J. M. Nichol, S. P. Harvey, M. D. Shulman, A. Pal, V. Umansky, E. I. Rashba, B. I. Halperin, and A. Yacoby, Nat. Commun. **6**, 7682 (2015).
[15] M. Pioro-Ladrière, J. H. Davies, A. R. Long, A. S. Sachrajda, L. Gaudreau, P. Zawadzki, J. Lapointe, J. Gupta, Z. Wasilewski, and S. Studenikin, Phys. Rev. B **72**, 115331 (2005).
[16] J. M. Elzerman, R. Hanson, J. S. Greidanus, L. H. Willems van Beveren, S. De Franceschi, L. M. K. Vandersypen, S. Tarucha, and L. P. Kouwenhoven, Phys. Rev. B **67**, 161308 (2003).
[17] A. Brataas and E. I. Rashba, Phys. Rev. B **84**, 045301 (2011).
[18] I. Neder, M. S. Rudner, H. Bluhm, S. Foletti, B. I. Halperin, and A. Yacoby, Phys. Rev. B **84**, 035441 (2011).
[19] J. R. Petta, A. C. Johnson, A. Yacoby, C. M. Marcus, M. P. Hanson, and A. C. Gossard, Phys. Rev. B **72**, 161301 (2005).
[20] We measure tunneling rates by applying square waves of different frequencies to the high bandwidth gates and monitoring charge transfer in/out of the dots. Because of the fast rise times of the square waves and the bandwidth limitations of our gates, the upper bound for our tunneling rate measurement is 20 MHz.
[21] G. Granger, G. C. Aers, S. A. Studenikin, A. Kam, P. Zawadzki, Z. R. Wasilewski, and A. S. Sachrajda, Phys. Rev. B **91**, 115309 (2015).
[22] D. Taubert, M. Pioro-Ladrière, D. Schröer, D. Harbusch, A. S. Sachrajda, and S. Ludwig, Phys. Rev. Lett. **100**, 176805 (2008).
[23] C. Barthel, D. J. Reilly, C. M. Marcus, M. P. Hanson, and A. C. Gossard, Phys. Rev. Lett. **103**, 160503 (2009).
[24] M. D. Shulman, O. E. Dial, S. P. Harvey, H. Bluhm, V. Umansky, and A. Yacoby, Science **336**, 202 (2012).
[25] E. A. Laird, J. M. Taylor, D. P. DiVincenzo, C. M. Marcus, M. P. Hanson, and A. C. Gossard, Phys. Rev. B **82**, 075403 (2010).
[26] G. C. Aers, S. A. Studenikin, G. Granger, A. Kam, P. Zawadzki, Z. R. Wasilewski, and A. S. Sachrajda, Phys. Rev. B **86**, 045316 (2012).